Frontiers in Heat and Mass Transfer

Tech Science Press

https://doi.org/10.32604/fhmt.2026.082479

ARTICLE

# $In_3SbTe_2$-Based Wideband Radiator with Gradient Emittance and Low Solar Absorptance

**Yang Long**[1], **Bowei Xie**[2,*], **Linkang Wang**[1] **and Mu Du**[2,*]

[1]Department of Mechanical and Electrical Engineering, Jiangxi Water Resources Institute, Nanchang, China
[2]Institute for Advanced Technology, Shandong University, Jinan, China

*Corresponding Authors: Bowei Xie. Email: xiebowei@sdu.edu.cn; Mu Du. Email: dumu@sdu.edu.cn

Received: 17 March 2026; Accepted: 26 May 2026; Published: 31 August 2026

**ABSTRACT:** This work proposes a simple multilayer smart coating with wide-band response characteristics based on $In_3SbTe_2$ (IST) phase change material, which can achieve significant and gradient dynamic regulation of infrared emittance while ensuring a low solar absorptance. The spectral directional emittance and absorptance characteristics are calculated by the rigorous coupled wave analysis method, and the genetic algorithm is used for global optimization design of the structural parameters. The simulated results show that the smart coating can maintain excellent optical performance with a solar absorptance lower than 0.325, while achieving a significant regulation range of infrared emittance over 0.80. This excellent radiation characteristic is primarily attributable to the interference effect of the FP resonant cavity and the multiple reflection mechanism of the multilayer film structure. The smart coating has been demonstrated to retain its the low solar absorptance and significant regulation of infrared emittance under different polarization states and large incident angles. Through the regulation of crystallinity parameters within the IST phase-change layer, continuous and stepwise modulation of thermal emittance can be realized, which markedly improves the dimension and flexibility of radiative property control. A quantitative analysis of the intelligent coating reveals that it possesses excellent radiation heat flow regulation capability. Its net radiation heat flux density can be dynamically adjusted from −400 to 600 $W/m^2$ within the temperature range of 250 to 330 K. Benefiting from its outstanding radiative properties and tunable regulation performance, the proposed smart coating exhibits promising application potentials in intelligent building energy conservation systems and aerospace thermal control fields, thereby laying a solid theoretical foundation for the development of novel intelligent thermal management technologies.

**KEYWORDS:** Smart coating; IST; gradient emittance; FP resonance; multiple reflection

## 1 Introduction

Smart coatings represent a significant innovation within the domain of building energy conservation, effecting a paradigm shift in the energy management model of buildings through their capacity to dynamically respond to environmental changes [1–3]. The fundamental value of the smart coating lies in the breakthrough of materials science, which has enabled the building envelope to possess autonomous perception and regulation capabilities. It has been observed to exhibit a radiative cooling state (high infrared emittance, low solar absorptivity) at high temperatures and switch to an insulation state (low infrared emittance) at low temperatures. The smart coating has been demonstrated to overcome the static limitations of traditional insulation materials, whilst also achieving synergy with the building equipment system. This results in the formation of a closed-loop energy-saving ecosystem. The application of smart coatings to buildings has been demonstrated to engender a substantial reduction in energy consumption throughout the life cycle of the building, whilst concomitantly extending the lifespan of the building envelope. Its significance is evident not only in its direct contribution to energy savings but also in its role as a pivotal technological catalyst for the construction industry's transition towards a zero-carbon agenda.

The realization of smart coatings is primarily contingent on phase change materials, and is achieved through particle composite structures [4], photonic crystal structures [5], and periodic micro-nano structures [6]. Xie et al. [5] proposed a multi-FP resonant cavity structure based on a $VO_2$, which has the capacity to achieve the superposition of multiple resonance peaks, thereby significantly enhancing the control range of infrared emission rate. Concurrently, a spacecraft thermal control coating with both low solar absorption and significant infrared modulation was proposed, in combination with the DBR multi-layer structure [7]. Araki and Zhang [8] proposed an adaptive thermal radiation control coating based on $VO_2$ nanowire structure, which can provide a total cooling power of 271 $W/m^2$ at high temperatures. Pal and Kim [9] prepared a flexible composite metamaterial coating by randomly dispersing $VO_2$ and ITO particles into PE, which was capable of achieving a regulation of the emittance ranging from 60% to 75%. Mandal et al. [10] developed a porous polymer coating capable of regulating the optical transmittance in accordance with the reversible wetting of any liquid. The device has been demonstrated to achieve transmittance ratios of 0.74 and 0.80 in the solar and visible light bands, respectively. Sun et al. [11] developed a patterned $VO_2$ ultrathin film thermal emission coating, which exhibits a high optical transmittance of 62% and an infrared emittance control of 0.26. This provides a novel method for space and ground radiation cooling thermal management. Kort-Kamp et al. [12] proposed a nano-photonic constant-temperature device multi-layer design based on $VO_2$. When the temperature is lower than the phase transition temperature, the multi-layer structure absorbs solar radiation and consequently heats up. However, when the temperature exceeds the phase transition temperature, the substance undergoes a process of electromagnetic energy emission through the atmospheric window, thereby releasing the energy into outer space. Ramirez-Cuevas et al. [13] pointed out that non-spherical antennas (e.g., rods, stars, sheets) composed of vanadium dioxide can demonstrate a substantial (approximately 200-fold) augmentation in absorption cross-section with an increase in temperature. The encapsulation of these antennas within polymer films, or the simple spraying of them to prepare a composite material, has been demonstrated to yield excellent control over the infrared emittance ($\Delta\varepsilon \sim 0.6$). Currently, smart coatings typically use $VO_2$ as the phase change material, which can only achieve two-level regulation of high and low emittance. This is insufficient to meet the requirements of complex climate changes. Kousis et al. [14] proposed a Passive Colored Radiative Coolers with a triple heat-rejection mechanism involving moderate solar reflectance, high infrared emissivity, and sunlight-excited fluorescence was the objective of this study. The purpose of this development was to effectively alleviate the glare, poor aesthetics, and winter overcooling issues inherent in conventional passive daytime radiative coolers, while achieving stable year-round thermal performance.

This work puts forward a proposal for a wide-band smart coating based on the $In_3SbTe_2$ (IST) phase-change material. This coating has the capacity to modulate gradient emittance while maintaining a low emittance. The coating is composed of an FP resonator cavity and a reflective reduction multilayer structure. The spectral directional emittance and absorptivity of the smart coating are calculated by the simulation using the Rigorous Coupled-Wave Analysis (RCWA) method, and the structural parameters of the smart coating are optimized using the Genetic Algorithm (GA). The present study investigates the influence of various structural parameters on the radiation characteristics of the smart coating, in addition to the variation of the absorptivity and emittance of the coating under different incident angles. The smart coating, based on IST, has the capacity to achieve stepwise changes in emittance and has significant application potential in fields such as building energy conservation, aerospace, and intelligent thermal management.

## 2 Theoretical Parts

Fig. 1 illustrates the scheme of the programmable wideband radiator. As shown in Fig. 1, the programmable wideband radiator is composed of ZnS/$CaF_2$ multiple stacks and IST/$CaF_2$/Al cavity. Fig. 2 shows the complex refractive index of the IST, ZnS and $CaF_2$. The $CaF_2$ and ZnS is transparent in the visible to infrared spectral range. The complex refractive index of $CaF_2$ and ZnS in Ref. [15], and IST in Ref. [16] are used in this work. The IST/$CaF_2$/Al cavity is FP cavity, which responses the emission and tunability of the radiator. The ZnS/$CaF_2$ multiple stacks acts as the AR and the spectral selective solar reflector, which can enhance the infrared emittance and reduce the solar absorptance. IST is a non-volatile thermal-induced phase-change material that has the capacity to transform from an amorphous state to a crystalline state. The two-phase optical properties of IST exhibit a high degree of contrast, facilitating the attainment of substantial radiation characteristic control. Furthermore, the phase state can be reliably sustained over an extended period, exhibiting high-speed cutting and low-power switching characteristics. The device has been demonstrated to be highly suitable for use in radiation characteristic control devices. Two strategies are proposed to gradient modulate the emittance of the radiator. As shown in Fig. 1, the first one is to utilize laser pulses to generate heating, thereby creating a grating-like micro-nano structure. The second one is the utilization of nucleation in partial crystalline state of IST. The optical response of IST can be continuously tuned by employing different energies on it or manipulating the baking time with the same heat level, thereby leading to formation of nucleation in partial crystalline state. Generally speaking, the changes of crystalline states can be achieved by thermal stimulus or laser pulse irradiation. To describe the effective permittivity $\varepsilon_{\text{eff}}$ of IST with various crystallization conditions, Lorentz-Lorenz relation can be employed [17].

$$\frac{\varepsilon_{\text{eff}}(\lambda)-1}{\varepsilon_{\text{eff}}(\lambda)+2}=m\frac{\varepsilon_{\text{cIST}}(\lambda)-1}{\varepsilon_{\text{cIST}}(\lambda)+2}+(1-m)\frac{\varepsilon_{\text{aIST}}(\lambda)-1}{\varepsilon_{\text{aIST}}(\lambda)+2} \quad (1)$$

where $\varepsilon_{\text{cIST}}$ and $\varepsilon_{\text{aIST}}$ are the permittivity of crystalline and amorphous IST, respectively. $m$ is the crystallization fraction of the IST, ranging from 0 to 1.

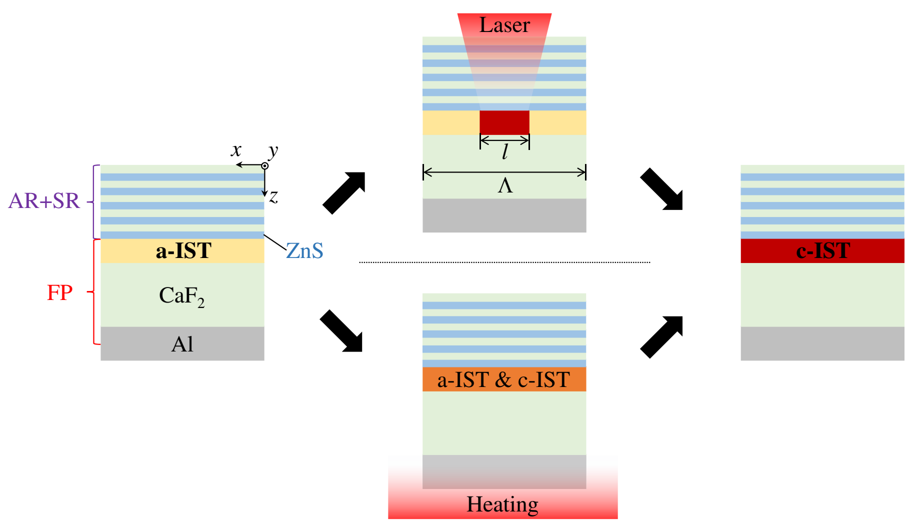


**Figure 1:** Scheme of the programmable wideband radiator.

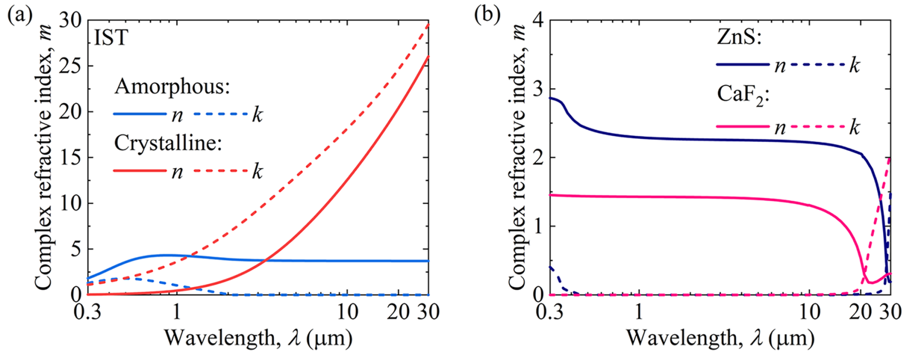


**Figure 2:** The complex refractive index of (**a**) IST [16], and (**b**) ZnS and CaF2 [15].

The spectral directional hemispherical reflectance was calculated by the RCWA method [18,19]. According to Kirchhoff's law, the spectral directional emittance $\varepsilon_{\lambda,\theta}$ of an opaque material can be expressed by

$$\varepsilon_{\lambda,\theta} = a_{\lambda,\theta} = 1 - R_{\lambda,\theta} \tag{2}$$

where $a_{\lambda,\theta}$ is the spectral directional absorptance, and $R_{\lambda,\theta}$ is the spectral directional hemispherical reflectance. $\theta$ is the angle of incidence, which is equal to zero at normal incidence. The total directional infrared emittance $\varepsilon_\theta$ is defined as the integration of the spectral directional emittance in the spectral range of 2.5~30 μm:

$$\varepsilon_\theta = \frac{\int_{2.5\mu\text{m}}^{30\mu\text{m}} \varepsilon_{\lambda,\theta} \mathrm{E}_{\mathrm{b}\lambda}(\lambda, T)\,\mathrm{d}\lambda}{\int_{2.5\mu\text{m}}^{30\mu\text{m}} \mathrm{E}_{\mathrm{b}\lambda}(\lambda, T)\,\mathrm{d}\lambda} \tag{3}$$

where $E_{\mathrm{b}\lambda}$ is the spectral emissive power of a blackbody at temperature $T$ of 300 K given by Planck's function. The total directional solar absorptance $a_\theta$ is defined as the integration of the spectral directional absorptance in the spectral range of 0.3~2.5 μm:

$$a_\theta = \frac{\int_{0.3\mu\text{m}}^{2.5\mu\text{m}} a_{\lambda,\theta} S_{\text{solar}}(\lambda)\,\mathrm{d}\lambda}{\int_{0.3\mu\text{m}}^{2.5\mu\text{m}} S_{\text{solar}}(\lambda)\,\mathrm{d}\lambda} \tag{4}$$

where $S_{\text{solar}}(\lambda)$ is the spectral solar radiant power. The spectral hemispherical emittance $\varepsilon_\lambda$ and the spectral hemispherical absorptance $a_\lambda$ is calculated by

$$\varepsilon_\lambda = a_\lambda = \frac{\int_{\Omega=2\pi} I_{\mathrm{b}\lambda}\varepsilon_{\lambda,\theta}\cos\theta d\Omega}{\int_{\Omega=2\pi} I_{\mathrm{b}\lambda}\cos\theta d\Omega} \tag{5}$$

where $I_{\mathrm{b}\lambda}$ is the spectral directional radiation intensity of blackbody.

The number of $BaF_2$/ZnSe pairs and thickness of each layer in the proposed smart radiator are optimized to achieve a low solar absorptance and high emittance tunability. The optimization is carried out through a retrieval process using Genetic Algorithm (GA) for the inverse problem and the RCWA method for the forward problem. In GA, the fitness function $F$ is the key parameter that determines the search direction of the optimization process, which is defined as

$$F(l_1, l_2, l_3 \ldots l_i) = 1 - (\varepsilon_{\text{normal,m}} - \varepsilon_{\text{normal},d}) + a_{\text{normal,m}} + a_{\text{normal},d} \tag{6}$$

where $l_i$ is the thickness of $i$th layer. $\varepsilon_{\text{normal,m}}$ and $\varepsilon_{\text{normal,d}}$ are the total normal infrared emittance for the metallic state and dielectric state, respectively, while $a_{\text{normal,m}}$ and $a_{\text{normal,d}}$ are the total normal solar absorptance for the metallic state and dielectric state, respectively.

The temperature $T$ and the net emitting/absorbing heat flux $Q_{\text{net}}$ of the all-season smart coating can be obtained by solving the heat balance equation [20–22]:

$$Q_{\text{net}} = Q_{\text{emit}}\left(T\right) - Q_{\text{atm}}\left(T_{\text{atm}}\right) - Q_{\text{parasitic}}\left(T, T_{\text{atm}}\right) - Q_{\text{sun}}\left(T\right) - Q_{\text{heat}} \tag{7}$$

where $T_{\text{amb}}$ is the ambient temperature. $Q_{\text{heat}}$ is the internal heat source flux. $Q_{\text{emit}}$ stands for the emitting heat flux from the smart coating expressed by

$$Q_{\text{emit}}\left(T\right) = A\int_{2\pi}\int_0^\infty E_{b\lambda}\left(T, \lambda\right)\varepsilon_{\lambda,\theta}\text{d}\lambda\cos\theta\text{d}\Omega \tag{8}$$

where $A$ represents the coating area, $E_{b\lambda}$ is the spectral emissive power of a blackbody at temperature $T$ given by Planck's function. The spectral directional emittance $\varepsilon_{\lambda,\theta}$ is dependent on the critical point of $VO_2$. Here, we assume that the phase transition of $VO_2$ occurs at the temperature of 290 K. $Q_{\text{atm}}$ is the absorbed heat flux due to the incident thermal radiation from atmosphere:

$$Q_{\text{atm}}\left(T_{\text{atm}}\right) = A\int_{2\pi}\int_0^\infty E_{b\lambda}\left(T_{\text{atm}}, \lambda\right)\varepsilon_{\lambda,\theta}\varepsilon_{\lambda,\theta}^{\text{atm}}\text{d}\lambda\cos\theta\text{d}\Omega \tag{9}$$

Here $\varepsilon_{\lambda,\theta}^{\text{atm}}$ is the absorptivity of the atmosphere, which can be calculated by $1 - \tau_{\text{atm}}(\lambda,\Omega)$. $\tau_{\text{atm}}(\lambda,\Omega)$ is the spectral atmosphere transitivity, which can be obtained from MODRAN5. $Q_{\text{parasitice}}$ is the parasitic heat flux due to conduction and convection:

$$Q_{\text{parasitic}}\left(T, T_{\text{atm}}\right) = Ah\left(T_{\text{atm}} - T\right) \tag{10}$$

where $h$ is the heat transfer coefficient. Here we consider $h$ = 8 W/(m$^2$·K) to mimic a typical natural air convection condition [22,23]. $Q_{\text{sun}}$ is the absorbed solar heat flux by the smart coating:

$$Q_{\text{sun}}\left(T\right) = A\int_0^\infty I_{\text{AM1.5}}\left(\lambda\right)\varepsilon_{\lambda,\theta}\text{d}\lambda \tag{11}$$

where $I_{\text{AM1.5}}$ represents the AM1.5 solar radiant power.

## 3 Result and Analysis

Fig. 3a illustrates the optimized objective function as a function of ZnS/$CaF_2$ pair number. Fig. 3b shows the changes in the total normal solar absorptance and total normal infrared emittance of the smart coating in the normal direction. As shown in Fig. 3, the objective function value exhibits a monotonically decreasing trend as the number of ZnS/$CaF_2$ stacks increases. However, when the number of ZnS/$CaF_2$ stacks exceeds 3, the decrease of the objective function becomes relatively gentle. It is evident that upon reaching a total of three ZnS/$CaF_2$ stacks, the modulation range of the normal solar absorptance and infrared emittance of the smart coating becomes uniform. The further optimization of the radiation characteristics of the coating is hindered by the ongoing increase in the number of stacks. Instead, this results in an increase in the number of coating layers, a more complex structure, and an increase in the preparation cost. In the subsequent part of this paper, the radiation characteristics and radiation heat flow of the intelligent coating with 3 stacks will be further elaborated.

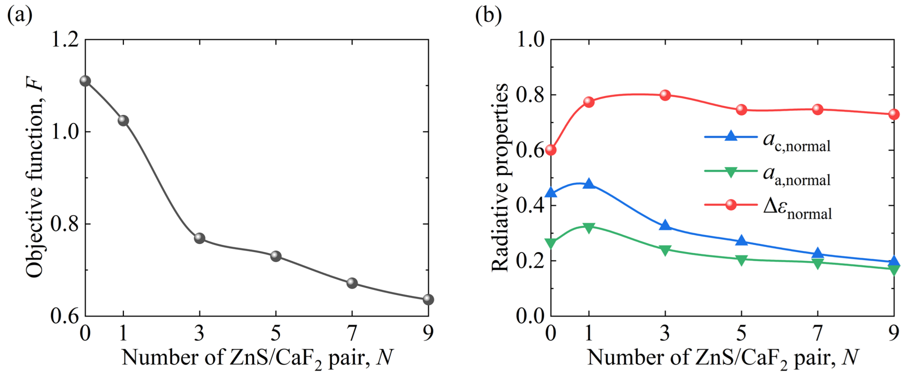


**Figure 3:** (**a**) The optimized objective function as a function of $ZnS/CaF_2$ pair number; (**b**) the optimized total normal solar absorptance and the infrared emittance tunability of the programmable wideband radiator with different $ZnS/CaF_2$ pair number.

Fig. 4 shows the spectral normal absorption rate of the intelligent coating in crystalline and amorphous states when the number of $ZnS/CaF_2$ stacks is equal to 3. As shown in Fig. 4, it has been demonstrated that within the infrared spectral range, IST exhibits a strong metallic property and has the capacity to form an $IST/CaF_2/Al$ FP resonant cavity. This resonant cavity has the capacity to enhance the absorption/emission of the coating to a significant degree. However, in the case of IST in an amorphous state, a transparent state is exhibited in the infrared band, as illustrated in Fig. 2a. Consequently, the smart coating demonstrates low emission characteristics. In the solar spectral range, the smart coating exhibits minimal absorption, irrespective of its crystalline or amorphous state. This phenomenon is attributable to the selective transmission and reflection characteristics of the DBR multilayer structure. The spectral emittance curves of the smart coating, in both crystalline and amorphous states, demonstrate strong oscillations, which are attributed to multiple reflections within the FP resonant cavity and the DBR structure.

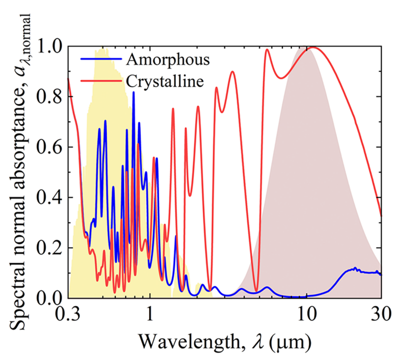


**Figure 4:** The spectral normal absorptance of the programmable wideband radiator with 3 $ZnS/CaF_2$ pairs for amorphous and crystalline state.

Fig. 5 presents the cloud map of the spectral directional emittance of the smart coating under different polarized light incidences. As demonstrated in Fig. 5a,b, in the amorphous state, the smart coating displays minimal solar absorptance and low infrared emittance under both TM and TE wave incidence. The crystalline smart coating has been demonstrated to exhibit a low solar absorptance and a high infrared emittance when subjected to both TM and TE wave incidence. Notably, even at incident angles of considerable magnitude, the smart coating exhibits the capacity to preserve its inherent property of minimal solar absorption, whilst concurrently demonstrating an augmented capacity for adjustment in terms of infrared emittance. Fig. 6 shows the hemispherical spectral absorptance of the smart coating is evident in both the crystalline and amorphous states. As demonstrated in Fig. 6, the hemispherical spectral absorption rate of the intelligent coating continues to manifest a substantial regulatory characteristic within the infrared spectrum range, remaining at a comparatively modest value within the solar spectrum range. It can thus be concluded that the radiation characteristics and adjustable amplitude of the proposed multilayer smart coating are almost unaffected by the polarization state of the incident wave and the incident angle.

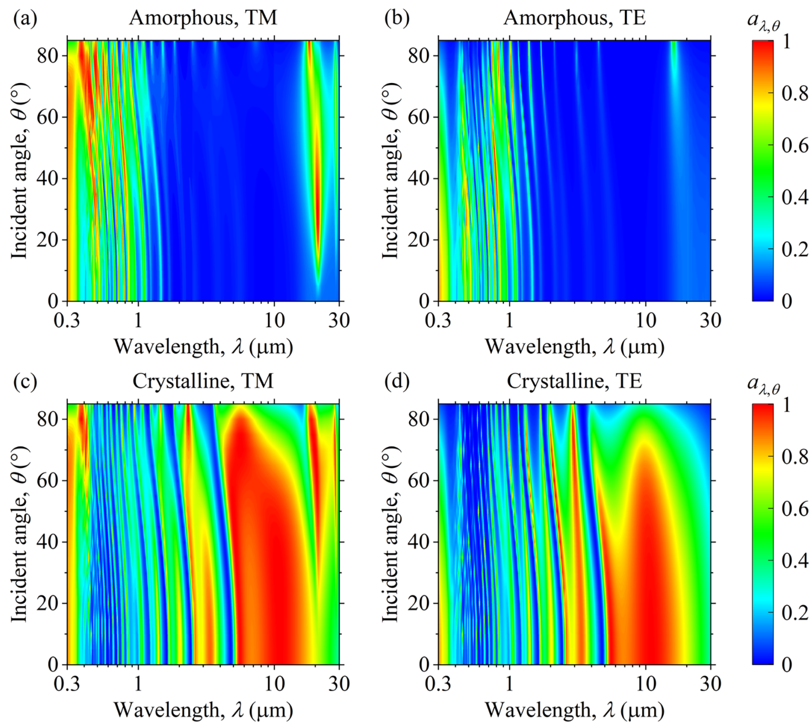


**Figure 5:** Cloud maps of spectral directional absorptance of the smart coating: (**a**) amorphous state, TM wave; (**b**) amorphous state, TE wave; (**c**) crystalline state, TM wave; (**d**) crystalline state, TE wave.

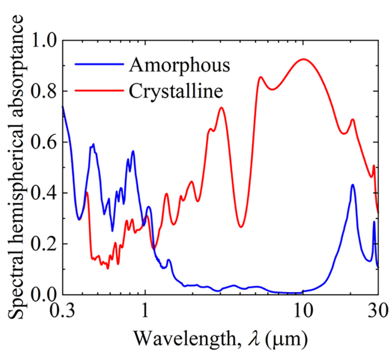


**Figure 6:** The hemispherical spectral absorptance of the smart coating.

Fig. 7 shows the variation patterns of the normal total solar absorptance and infrared emittance of the smart coating under different grating periods Λ with respect to the percentage of different crystal states. The regulation of the crystal percentage in the figure is achieved by changing the width *l* of the rectangular grating, without altering the crystallinity of the IST layer. As demonstrated in Fig. 7a, with an augmentation in the width *l* of the rectangular grating, the normal total solar absorptance of the smart coating exhibits an initial increase, followed by a subsequent decrease. Concurrently, as the grating period increases, the infrared emittance of the smart coating demonstrates a gradually decreasing trend. However, it should be noted that, in the case of IST, the percentage of crystalline phase has only a relatively minor influence on the normal total solar absorptance of the smart coating. This phenomenon can be attributed to the relatively minor alteration in the complex refractive index of IST prior to and following the phase transition within the solar spectrum. In the case of crystalline IST, the period and width of the rectangular grating have been shown to have a very significant impact on the normal total infrared emittance in the infrared band. As demonstrated in Fig. 7b, the normal total infrared emittance of the smart coating exhibits a substantial increase with an increase in the period and width of the rectangular grating. Specifically, when the grating period is large, the infrared emittance increases rapidly at first and then tends to level off as the grating width increases; conversely, when the grating period is small, the opposite occurs. In the crystalline state, IST exhibits a strong metallic property, which is conducive to the formation of a stronger FP resonance, leading to an increase in infrared emittance.

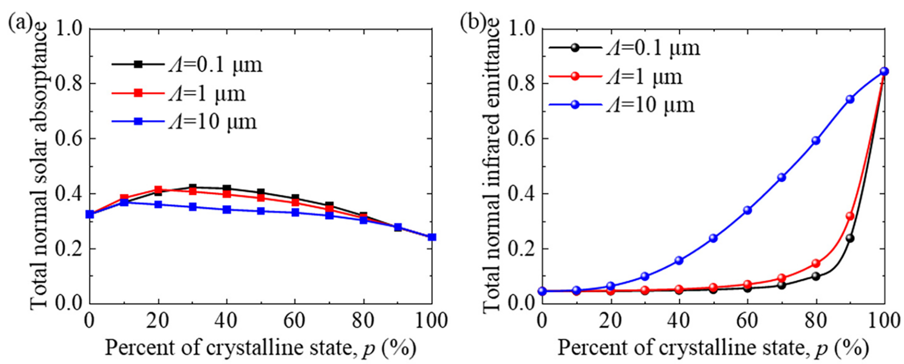


**Figure 7:** The normal total (**a**) solar absorptance and (**b**) infrared emittance of the smart coating with a nanograting structure as a function of the percent of crystalline state. The modulation of the crystalline fraction in the figure is achieved by changing the length *l* of the rectangular grating, without altering the crystallinity of the IST layer.

Fig. 8 shows the variation patterns of the normal total solar absorptance and infrared emittance of the smart coating with different percentages of crystalline state. The control of the crystalline percentage in the figure is achieved by modifying the crystallinity of the IST layer, without altering the structure of the smart coating. As demonstrated in Fig. 8, the solar absorptance of the smart coating initially increases and subsequently decreases as the crystallinity of the IST increases. However, the overall trend is relatively gentle, which is analogous to the phenomenon observed in Fig. 7a. The infrared emittance of the smart coating is known to increase with the increase in the crystallinity of the IST. In instances where crystallinity is comparatively low, the change is gentle, whilst in cases where crystallinity is high, there is a sharp rise. This phenomenon can be elucidated by the necessity of the IST layer exhibiting strong metallic properties for the formation of FP resonance. It is important to note that, while the infrared emittance is subject to significant regulation, the solar absorptance also varies among the different phases. The solar absorptance of the samples exhibited a transition from 0.325 in the amorphous state to 0.242 in the crystalline state, with a relatively negligible difference between the two states. This is due to the fact that, during the process of optimization, the objective function necessitates that the solar absorptance be minimized in both phases.

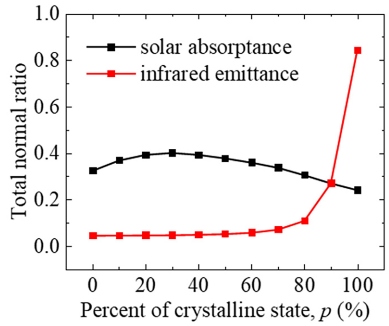


**Figure 8:** The normal total solar absorptance and infrared emittance of the smart coating as a function of the percent of crystalline state. The modulation of the crystalline percentage in the figure is achieved by altering the crystallinity of the IST layer without changing the structure of the smart coating.

IST is a temperature-change-driven non-volatile phase-change material that has the capacity to generate rapid temperature variations through electrical, thermal or optical stimulation, with an extremely fast phase transition time. It is evident that, due to its non-volatile property, both phase states can be stably maintained for a considerable duration. Fig. 9 presents the radiation heat flow curves of the smart coating in (a) crystalline state and (b) amorphous state, with the environmental temperature set at 280 K. The net radiation heat flow $Q_{net}$, total radiation heat flow $Q_{cooler}$, absorbed atmospheric radiation heat flow $Q_{amb}$, heat flow absorbed from the surrounding environment through convection $Q_{parasitic}$, and absorbed solar radiation heat flow $Q_{sun}$ are all shown in the figure, with the internal heat source $Q_{heat}$ set to zero. When the smart film releases heat outward, its net heat flux is positive, which is called the radiation cooling mode; while when the smart film absorbs energy, its net heat flux is negative. When the IST is in the crystalline state, the smart coating exhibits significant solar heating capabilities, as demonstrated in Fig. 9a. It has been determined that at a temperature of 250 K, the net radiant heat flux of the coating in question exceeds −400 W/m2. Concurrently, the net radiant heat flux experiences a substantial increase with rising temperature, primarily attributable to diminished convective heat absorption. As demonstrated in Fig. 9b, when the temperature exceeds 285 K, the smart coating in the crystalline state of IST can transition to a radiation cooling mode. It is evident that the net radiant cooling heat flux undergoes a substantial increase with an escalation in temperature, attaining a magnitude of 600 $W/m^2$ at 330 K. This phenomenon can be ascribed to the markedly augmented total radiant heat flux that accompanies an increase in temperature. In summary, the smart coating exhibits excellent control characteristics, capable of achieving insulation and even solar heating properties at low temperatures by using amorphous IST, and achieving excellent radiation cooling properties based on crystalline IST at high temperatures.

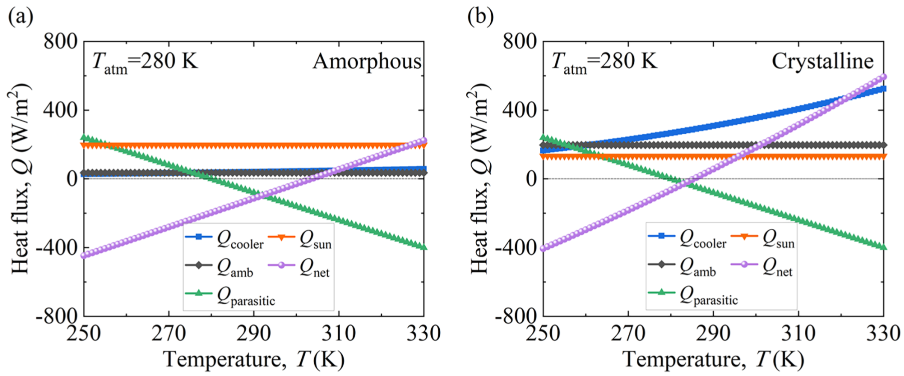


**Figure 9:** Radiation heat flux of the smart coating in (**a**) crystalline state and (**b**) amorphous state.

## 4 Conclusion

This work proposes a wide-band smart coating based on IST phase-change materials, which can achieve gradient modulation of infrared emittance while maintaining a low solar absorptance. The coating consists of a FP resonator cavity and a reflective multilayer structure. The spectral directional emittance and absorptance of the smart coating are calculated using the RCWA method, and the structural parameters of the smart coating are optimized using GA. The results show that the smart coating can achieve a significant modulation of infrared emittance ($\Delta\varepsilon > 0.80$) while maintaining a low solar absorption rate ($a < 0.36$). This excellent radiation property is mainly due to the FP resonance and multiple reflections. The smart coating still maintains this low solar absorption and significant infrared emittance modulation characteristics under different polarization states and large angles of incidence. Based on the change in the crystallinity of the IST layer, the emittance of the smart coating can be regulated in a stepwise manner, greatly enriching the diversity and flexibility of the modulation. At the same time, the modulation ability of the smart coating on the radiant heat flux is quantitatively demonstrated, with the net radiant heat flux ranging from −400 W/m$^2$ at 250 K to 600 W/m$^2$ at 330 K. Due to its excellent radiation properties, the smart coating has significant application potential in smart buildings and aerospace fields.

**Acknowledgement:** Not applicable.

**Funding Statement:** The authors received no specific funding for this study.

**Author Contributions:** The authors confirm contribution to the paper as follows: Conceptualization, Bowei Xie; methodology, Yang Long and Bowei Xie; software, Yang Long and Bowei Xie; validation, Yang Long and Bowei Xie; formal analysis, Yang Long and Linkang Wang; investigation, Yang Long and Linkang Wang; resources, Bowei Xie; data curation, Yang Long and Linkang Wang; writing—original draft preparation, Yang Long; writing—review and editing, Bowei Xie and Mu Du; visualization, Yang Long and Bowei Xie; supervision, Mu Du; project administration, Bowei Xie; funding acquisition, Bowei Xie and Mu Du. All authors reviewed and approved the final version of the manuscript.

**Availability of Data and Materials:** Data available on request from the authors. The data that support the findings of this study are available from the Corresponding Author, Mu Du, upon reasonable request.

**Ethics Approval:** Not applicable.

**Conflicts of Interest:** The authors declare no conflicts of interest.

## References


1. Annual report 2020. London, UK: World Green Building Council; 2020. p. 14–5.
2. Global status report for buildings and construction 2023. Nairobi, Kenya: The UNEP-hosted Global Alliance for Buildings and Construction; 2023. p. 9.
3. Henry A, Prasher R, Majumdar A. Five thermal energy grand challenges for decarbonization. Nat Energy. 2020;5(9):635–7. doi:10.1038/s41560-020-0675-9.
4. Xie B, Dong J, Zhao J, Liu L, Fu X, Zhai Z. $VO_2$ particle-based intelligent metasurface with perfect infrared emission for the spacecraft thermal control. Appl Opt. 2022;61(35):10538. doi:10.1364/ao.475672.
5. Xie B, Zhang W, Zhao J, Liu L. VO2-based superposed Fabry-Perot multilayer film with a highly enhanced infrared emittance and emittance tunability for spacecraft thermal control. Opt Express. 2022;30(19):34314. doi:10.1364/oe.464266.
6. Tang K, Dong K, Li J, Gordon MP, Reichertz FG, Kim H, et al. Temperature-adaptive radiative coating for all-season household thermal regulation. Science. 2021;374(6574):1504–9. doi:10.1126/science.abf7136.
7. Xie B, Zhang W, Zhao J, Zheng C, Liu L. Design of $VO_2$-based spacecraft smart radiator with low solar absorptance. Appl Therm Eng. 2024;236:121751. doi:10.1016/j.applthermaleng.2023.121751.
8. Araki K, Zhang RZ. An optimized self-adaptive thermal radiation turn-down coating with vanadium dioxide nanowire array. Int J Heat Mass Transf. 2022;191:122835. doi:10.1016/j.ijheatmasstransfer.2022.122835.
9. Pal SK, Kim G. Scalable and flexible radiative cooling composite metamaterial structure with thermally responsive emissivity tunability. Compos Part B Eng. 2025;295:112207. doi:10.1016/j.compositesb.2025.112207.
10. Mandal J, Jia M, Overvig A, Fu Y, Che E, Yu N, et al. Porous polymers with switchable optical transmittance for optical and thermal regulation. Joule. 2019;3(12):3088–99. doi:10.1016/j.joule.2019.09.016.
11. Sun K, Xiao W, Wheeler C, Simeoni M, Urbani A, Gaspari M, et al. $VO_2$ metasurface smart thermal emitter with high visual transparency for passive radiative cooling regulation in space and terrestrial applications. Nanophotonics. 2022;11(17):4101–14.
12. Kort-Kamp WJM, Kramadhati S, Azad AK, Reiten MT, Dalvit DAR. Passive radiative "thermostat" enabled by phase-change photonic nanostructures. ACS Photonics. 2018;5(11):4554–60. doi:10.1021/acsphotonics.8b01026.s002.
13. Ramirez-Cuevas FV, Gurunatha KL, Li L, Zulfiqar U, Sathasivam S, Tiwari MK, et al. Infrared thermochromic antenna composite for self-adaptive thermoregulation. Nat Commun. 2024;15(1):9109. doi:10.1038/s41467-024-53177-6.
14. Kousis I, Khan HS, Paolini R, Webb JEA, Valenta J, Santamouris M. Cooling with colour: passive-coloured radiative coolers for energy-efficient temperature regulation in adverse climatic conditions. Sol Energy. 2025;290(7):113343. doi:10.1016/j.solener.2025.113343.
15. Palik ED. Handbook of optical constants of solids. Cambridge, MA, USA: Academic Press; 1985.
16. Heßler A, Wahl S, Leuteritz T, Antonopoulos A, Stergianou C, Schön CF, et al. $In_3SbTe_2$ as a programmable nanophotonics material platform for the infrared. Nat Commun. 2021;12:924. doi:10.1117/12.2594188.
17. Aspnes DE. Local-field effects and effective-medium theory: a microscopic perspective. Am J Phys. 1982;50(8):704–9. doi:10.1119/1.12734.
18. Moharam MG, Gaylord TK. Rigorous coupled-wave analysis of planar-grating diffraction. J Opt Soc Am. 1981;71(7):811. doi:10.1364/josa.71.000811.
19. Moharam MG, Gaylord TK, Grann EB, Pommet DA. Formulation for stable and efficient implementation of the rigorous coupled-wave analysis of binary gratings. J Opt Soc Am A. 1995;12(5):1068. doi:10.1364/josaa.12.001068.
20. Raman AP, Abou Anoma M, Zhu L, Rephaeli E, Fan S. Passive radiative cooling below ambient air temperature under direct sunlight. Nature. 2014;515(7528):540–4. doi:10.1038/nature13883.
21. Zhai Y, Ma Y, David SN, Zhao D, Lou R, Tan G, et al. Scalable-manufactured randomized glass-polymer hybrid metamaterial for daytime radiative cooling. Science. 2017;355(6329):1062–6. doi:10.1126/science.aai7899.
22. Zhao D, Aili A, Zhai Y, Xu S, Tan G, Yin X, et al. Radiative sky cooling: fundamental principles, materials, and applications. Appl Phys Rev. 2019;6(2):021306. doi:10.1063/1.5087281.
23. Zhao D, Aili A, Zhai Y, Lu J, Kidd D, Tan G, et al. Subambient cooling of water: toward real-world applications of daytime radiative cooling. Joule. 2019;3(1):111–23. doi:10.1016/j.joule.2018.10.006.